Pattern formation of granular avalanches with vortex convection

Hirofumi Niiya, Akinori Awazu, and Hiraku Nishimori
Department of Mathematical and Life Sciences, Hiroshima University, Higashihiroshima 739-8526, Japan
(Dated: February 7, 2013)

It has been known that the granular flow of polystyrene particles down a slope forms a wavy pattern with many heads at the moving front of the resulting avalanche. In experiments of granular flow using low-density particles, the instability of the moving front and the subsequent head formation are driven by gravity and air drag. To elucidate the instability mechanism of granular avalanches, we propose a particle method considering gravity as the driving force for the avalanche, the contact interaction between granular particles, and the long-range interaction between granular particles through the ambient fluid as a type of air drag. Using this model, we simulate the head formation at the moving front of the avalanche, and we investigate the particle flow caused by the air drag. It is found that the air drag destabilizes the shape of the avalanche that deforms into a wavy pattern, leading to the generation of a pair of granular vortex convection currents inside the head. Further, the relationship between the particle radius and head size is found to satisfy the positive linear scaling law. Moreover, the hydrodynamic interaction between the particles causes their aggregation at the moving front of the avalanche, and this aggregation effect generates the head-tail structure. These numerical results are qualitatively consistent with the results of previous experiments.

Avalanches, generally taken as a class of massive landslide phenomena, involve gravity currents and density currents, for instance, snow avalanches, debris flows, and pyroclastic flows. These flows slide down a slope as a mixture of solid and fluid and form several kinds of typical structures, one of which is termed as the head-tail structure [1–7]. Concretely, at the moving front of an avalanche, a large head is formed through the clustering of large particles, whereas at the rear end, an elongated tail is formed by the trailing smaller particles. Among potential factors for the formation of the head-tail structure, the ratio of air drag to gravity is considered as the most relevant. For example, a granular flow consisting of low-density particles such as polystyrene particles forms the head-tail structure as well as the wavy pattern with many heads at the moving front of the avalanche [8]. In addition, these experiments show that the positive linear relation between head size and particle radius is a rough approximation. In contrast, experiments using high-density particles such as glass beads do not generate the head-tail structure, although they form a wavy pattern similar to that obtained when using low-density particles [2]. This difference in the formation of the avalanche structure due to the difference in particle density can be estimated based on whether or not the air drag efficiently acts on the particles [9].

In order to explain these facts by theoretical means, several models have recently been proposed; the fluid flow model assumes an avalanching body as a mass of fluid, the mass center model assumes an avalanche as a huge single particle, and so on [10–14]. However, the materials constituting avalanches that are used in these models are granular materials such as polystyrene or glass beads, which are definitely not fluid. Moreover, the single particle model does not treat the interaction between granular particles, which is speculated to play a crucial role in the dynamics of an avalanche. To overcome the above shortcomings these models, we employ a particle method considering the contact between granular particles and the fluid effect as the air drag. In this study, we investigate the head formation in a granular avalanche by considering the particle radius, and we clarify the instability mechanism of granular avalanches, which leads to the generation of the head.

In our model, a granular flow slides down a slope that is steeper than the angle of repose, and this model is roughly based on three basic assumptions: First, the granular flow consisting of spherical (three-dimensional) particles only moves along either a 2D inclined slope or a 2D vertical cross-section extending over a slope. Second, only the translational motion of particles along either of the two 2D spaces is considered, that is, the rotational motion of particles is ignored. Third, as regards the main force acting on the particles, we consider three types of forces: (i) gravity as the dominant driving force for the avalanche, (ii) the repulsive force between particles that is caused by the excluded volume effect, and (iii) the drag force due to the fluid. The specific form of each force is described as below.

(i) Gravity: Considering the density difference between the granular particles and the fluid, the gravity of the ith particle $\mathbf{F}_{gi}$ is expressed as

$$\mathbf{F}_{gi} = -e_y V_i g(\rho_p - \rho_f),$$

where e_y denotes the unit vector parallel to the y-axis, V_i denotes the volume of the ith particle, g denotes the gravitational acceleration, and ρ_p and ρ_f denotes the densities of the particle and the fluid, respectively.

(ii) Repulsive force: We ignore the rotational motion of the particles, and we assume that the ith particle experiences only a normal directional force $\mathbf{F}_{ri}$, which acts as the repulsive force caused by contact with the jth par-

ticle and is represented as the elastic spring force

$$\mathbf{F}_{ri} = -e_{\theta(i,j)} k_n \delta, \;\; e_{\theta(i,j)} = \begin{pmatrix} \cos\theta_{(i,j)} \\ \sin\theta_{(i,j)} \end{pmatrix},$$

where $\theta_{(i,j)}$ denotes the relative angle of $\mathbf{r} = \mathbf{r}_j - \mathbf{r}_i$ to the positive direction of the x-axis, where $\mathbf{r}_i$ and $\mathbf{r}_j$ represent the respective central coordinates of the ith and jth particles, k_n denotes the spring constant, and δ denotes the overlap distance between two particles. Here, δ is expressed in terms of the particle radius a and the interparticle distance $r = \sqrt{(x_i - x_j)^2 + (y_i - y_j)^2}$ as

$$\delta = \begin{cases} a_i + a_j - r & (r < a_i + a_j; \text{contact}) \\ 0 & (\text{else; noncontact}). \end{cases}$$

(iii) Drag force by fluid: The long-range interaction between the particles though the fluid is experienced by individual particles as a type of air drag force. Consequently, we assume that the motion of each particle immediately propagates though the fluid, and we use the Rotne–Prager tensor $\mathbf{J}(\mathbf{r})$ [15] to denote the effective long-range interaction between particles. This tensor is the exact solution of the Stokes equation in cases in which the fluid contains spherical particles, and the specific form is expressed as

$$\mathbf{J}(\mathbf{r}) = \frac{1}{r}\left[\mathbf{I} + \frac{\mathbf{rr}}{r^2} + \frac{2}{3}\left(\frac{a_j}{r}\right)^2\left(\mathbf{I} - 3\frac{\mathbf{rr}}{r^2}\right)\right], \;\; (\mathbf{r} = \mathbf{r}_i - \mathbf{r}_j), \quad (1)$$

where $\mathbf{I}$ denotes the unit tensor. Here, Eq. (1) indicates the fluid effect caused by the jth particle on the ith particle, and $\mathbf{rr}$ in Eq. (1) denotes the matrix in which each element corresponds to the tensor $\mathbf{J}$; for instance, the tensor element $\mathbf{J}_{xy}$ is expressed as $(\mathbf{rr})_{xy} = (x_i - x_j)(y_i - y_j)$.

Moreover, by ignoring the particle inertia and only considering the three abovementioned effects, the ith particle velocity $\mathbf{v}_i$ is determined as

$$\mathbf{v}_i = \frac{\mathbf{F}_i}{6\pi\mu a_i} + \sum_{j\neq i}^{N} \mathbf{u}_i(j) \quad (2)$$

$$\mathbf{u}_i(j) = \frac{1}{8\pi\mu}\mathbf{J}(\mathbf{r}) \cdot \mathbf{F}_j,$$

where $\mathbf{F}_i = \mathbf{F}_{gi} + \mathbf{F}_{ri}$, μ denotes the viscosity coefficient of the fluid, and $\mathbf{u}_i(j)$ denotes the induced velocity generated by the jth particle. Further, the first term in Eq. (2) is the expression for Stokes' drag formula.

Numerical simulations of the particle model are conducted on a flat slope with a constant inclination angle ($\theta = 45°$), where particles are confined in two different kinds of two-dimensional planes depending on model (Fig. 1): model-I) particles move along the 2D surface of the slope, and model-II) particles move within the 2D vertical cross-section extending over the slope. It is to be noted that model-I addresses the instability to generate wavy pattern at the moving front of an avalanche from the top-view perspective, where the effect of the inclination angle is reflected in the gravity term as $g\sin\theta$ and the friction between the particle and the slope is ignored. In contrast, model-II focuses on the head-tail structure formation and assumes that the collision of particles with the slope is described as the elastic spring force in a manner similar to the force involved in the collision between particles.

As regards the specific materials of the granular particle and fluid, we select a low-density particle such as polystyrene with the choice of the fluid as air for the purpose of experimental comparison. Concretely, the density ρ_p and the spring constant k_n of the granular particle are given as $\rho_p = 20$ kg m^{-3} and $k_n = 10$ N m^{-1}, respectively, whereas the density ρ_f and the viscosity coefficient μ of the fluid are fixed as $\rho_f = 1.2$ kg m^{-3} and $\mu = 1.82 \times 10^{-5}$ Pa s, respectively. As the control parameter, we vary only the particle radius a_p in the range of the order of millimeters, that is,

$$a_p = (1 \pm 0.05)s \times 10^{-3}\,\text{m}$$
$$s = \{1.0, 2.5, 5.0\}\;(\text{small}, \text{medium}, \text{large}), \quad (3)$$

where s denotes the criteria radius. Each particle used for the calculations is randomly selected within the range $[0.95 \times s, 1.05 \times s]$ to avoid crystallization of the particles. Further, both simulations of model-I and II are carried out 20 times with $N = 2000$ particles for different sets of particle radius and initial positions.

In model-I, we use two different configurations of the initial particle setup: i) circular setup (Fig. 2(a)) and ii) rectangular setup (Fig. 3(a)), which are introduced to focus on the formation of a single head and the structural instability at the moving front of avalanche, respectively. The spatial dimensions of both initial setups are chosen to be sufficiently large to pack $N = 2000$ particles into each setup depending on the criteria radius. Hence, the radius of the circular initial setup R and the lateral length of the rectangular initial setup L are set as $R = \{0.065, 0.17, 0.34\}$ and $L = \{0.35, 0.85, 1.7\}$ (small, medium, large), respectively. For the directional length of the slope of the rectangular initial setup, we fix the initial length as 10 particles. It is to be noted that the particles are randomly placed inside each setup, avoiding overlap between particles, and the packing fraction is nearly 0.5. In addition, the particle velocity v is derived

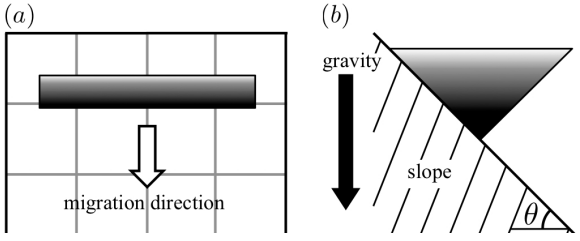

FIG. 1. Two different kinds of two-dimensional planes: (a) Model-I (top view), (b) Model-II (side cross-sectional view).

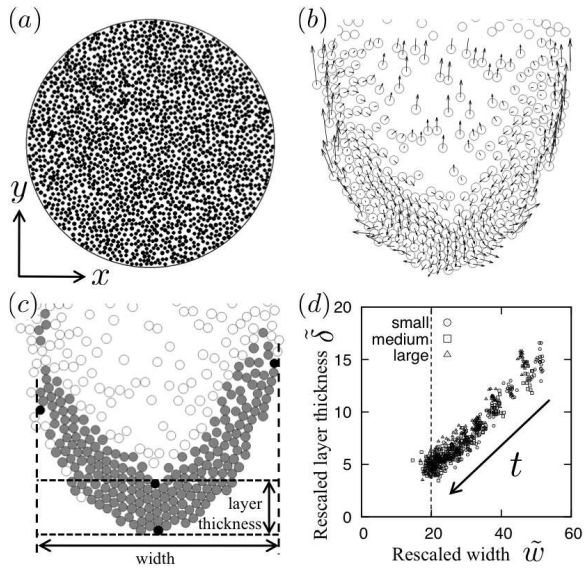

FIG. 2. Head formation for circular initial setup with $s = 5.0$; (a) $t = 0$ s. (b) Particle velocity field against migration speed of avalanche v_a at $t = 2.45 \times 10^{-3}$. The y component of the velocity vector is described as $v_y - v_a$, where v_y denotes the y component of the particle velocity. (c) Definition of width and layer thickness in head. The gray and black circles indicate the constituents of head and targets selected to measure head size, respectively. (d) Time evolutions of head size rescaled by criteria diameter.

from the particle model with a single particle as

$$v = \frac{2}{9}\frac{g\sin\theta(\rho_p - \rho_f)}{\mu}a_p^2. \tag{4}$$

Equation (4) indicates that the particle radius a_p strongly governs the particle velocity, and thus, numerical simulations are run until the simulation time reaches $t = 2\times10^{-2}, 10^{-2}, 5\times10^{-3}$ s (small, medium, large) depending on the criteria radius (Eq. (3)).

Next, we begin with the study of the head formation process using model-I with a circular initial setup. Initially, the particles are uniformly located within this setup (Fig. 2(a)), and they aggregate around the moving front as they travel down the slope, as described by Eq. (2); eventually, the aggregated particles form a single head. To observe the relative motion of particles at the head, we visualize the particles velocity relative to the mean migration speed of the head during the head formation. Figure 2(b) shows that the particles along the rear (upper) verge of the densely aggregated band of the head are pulled forward by the neighboring particles and move toward the center of the head, whereas the particles along the front (lower) verge of the head move away from the center of the head. In this manner, the granular avalanche migrates downward while a pair of granular vortices is maintained inside the head, through which process the head shrinks with time by leaving behind a certain portion of particles. It is to be noted that similar processes are observed independent of the criteria radius (Eq. (3)).

In order to measure the head size, we define the width w and layer thickness σ of the head as follows: First, to discern the head from the other structural parts of an avalanche, we choose particles according to the quantity

$$n_i' = \sum_{\substack{j\neq i \\ |\mathbf{r}_i-\mathbf{r}_j|<S_r}}^{N} \sum_{\substack{j\neq k \\ |\mathbf{r}_l-\mathbf{r}_k|<S_r}}^{N} 1,$$

where $S_r = 4 \times s$ denotes the search range. Here, n_i' indicates that the ith particle includes indirect neighbors through the jth particle, that is, n' yields the quasilocal particle number density. If the ith particle satisfies the condition $n_i' > n_{\max}'/4$, we select this particle as a constituent of the head, which is indicated as a gray (or black) circle in Fig. 2(c). Furthermore, we choose four target (i.e., black) particles within the head, which are located at the foremost position in the head, the forefront along the rear verge of the head, and the outmost positions in right and left arms of the head. According to the locations of these four black circles, we define the size of the head; the head width w is defined as the lateral length between the two outmost particles, whereas the head layer thickness δ is the slope directional length from the foremost particle to that along the rear verge in the head. The plot in Fig. 2(d) indicates that the head width shrinks with time to reach a finite width of about 20 particles during the simulation time independent of the criteria radius (Eq. (3)). Moreover, we found a strong positive correlation (correlation coefficient: 0.956) between the width $\tilde{w} = w/(2s)$ and the layer thickness $\tilde{\delta} = \delta/(2s)$ rescaled by the criteria diameter.

Next, the simulations using model-I with a rectangular initial setup show a time evolution in which the air drag destabilizes the initially straight front of the avalanche to deform into a wavy pattern with many heads (Figs. 3(a) and (b)). For this growth process of instability, we speculate that the dominant factor is the long-range fluid-mediated interaction between particles according to Eq. (1). This is because; the section of particles located around the middle height in the rectangular initial setup consist of a larger number of fluid-mediated interaction particles than those located near the verges of the setup; thus, the velocities of the former particles are larger than those of the latter, as reflected by the second term in Eq. (2). This velocity difference between the middle, frontal and rear particles gives rise to the aggregation of particles at the moving front of the avalanche as in the case of the circular initial setup. However, in this case of the laterally long initial setup, the randomness of the particle radius and initial inhomogeneity contributes to the subsequent evolution of the lateral inhomogeneity of the frontal pattern of the avalanche, which breaks down into a multi-head structure (Fig. 3(b)).

The heads in the wavy structure are characterized by a high particle number density, and we determine

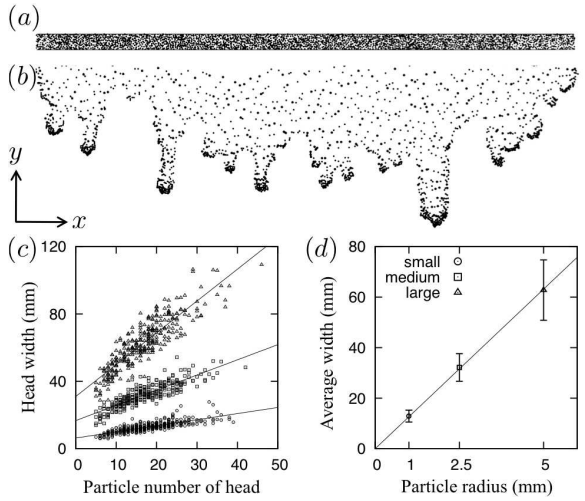

FIG. 3. Instability at moving front of avalanche for rectangular initial setup with $s = 5.0$; (a) $t = 0$ s and (b) $t = 3 \times 10^{-3}$ s. (c) Scatter diagram for particle number of head and head width. The solid line per criteria radius is obtained by the least square method. (d) Average width against particle radius. The vertical bars indicate absolute deviations, whereas the line passing through the origin is also fitted by the least square.

each head size according to the previously introduced approach (Fig. 2(a)). It is to be noted that numerical simulations with the circular initial setup were conducted for different time intervals depending on the criteria radius (Eq. (3)) such that the head sizes rescaled by the criteria diameter reached a certain value ($w' \approx 20$) during the simulation time (Fig. 2(d)). Further, in the second case of the simulations with the rectangular initial setup, the time interval of the simulations is set depending on the criteria radius such that the head formation is clearly observed, where the head size is measured at the end of the calculation. The mean numbers of emergent heads per simulation are 17.2, 13.95, and 14.85 (for small, medium, and large particles). The results in Fig. 3(c) indicate that the width of the head increases with the number of particles constituting the head (i.e. gray or black circles in Fig. 2(c)), and the relation between these two parameters can be roughly fitted by straight lines. To study the relation between the particle radius and the head size, we calculate the average width and obtain a linear relationship between the particle radius and the head width. These results quantitatively correspond to a previous experiment performed using polystyrene, and they show a similarity to the granular Rayleigh–Taylor instability observed in sedimenting suspensions [16, 17].

Finally, we establish whether model-II describing the granular avalanche in a vertical cross-section can reproduce the intrinsic head-tail structure for low-density granular particles. As the initial setup, the packing area of particles is prepared by a stopper extending perpendicular to the slope with inclination angle $\theta = 45°$ (Fig. 4(a)). The size of this packing area is given according to the vertical depth D, which is set as $D = \{0.115, 0.3, 0.6\}$ (small, medium, large) where the packing fraction is nearly 0.5. The numerical simulations show that the particles converge to the moving front of the avalanche via the long-range fluid-mediated interaction according to Eq. (1), and subsequently, the thickness of the front part becomes more than that of the rear part, that is, the granular avalanche forms the head-tail structure (Fig. 4(b)). Moreover, the head shrinks with time while retaining its structure because the particles located at the top of the head move backward.

In this study, we employed a particle method considering the fluid-mediated non-local particle-particle interaction using the Rotne–Prager tensor, and we investigated the pattern formation of granular avalanches in two different types of 2D space: (i) surface of constant slope and (ii) vertical cross-section extending over the slope. The numerical simulations using (i) showed that the fluid-mediated particle-particle interaction deforms the granular avalanches into a wavy pattern with many heads at the moving front. In addition, each head migrated downward while maintaining a granular vortex convection, for which the relation among particle radius, head thickness, and head width satisfied the linear scaling law. Moreover, the simulations using (ii) were successful in the reproduction of a characteristic head-tail structure independent of particle radius. These results qualitatively correspond to the results of previous experiments.

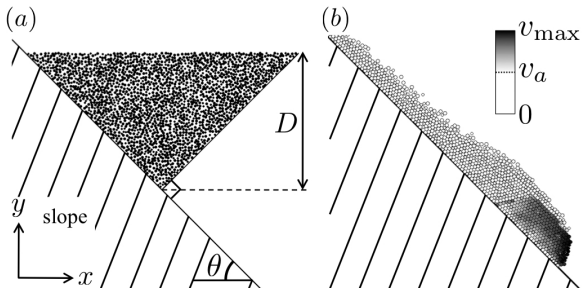

FIG. 4. Head-tail structure of avalanche in model-II with $s = 5.0$. (a) $t = 0$ s. D denotes the vertical depth of the packing area. (b) Particle velocity along slope at $t = 2 \times 10^{-3}$ s. The particles with velocities between the migration speed of avalanche v_a and maximum velocity $v_{\max}$ are characterized by the black color gradation.

[1] J. M. N. T. Gray, and K. Hutter, Continuum Mech. Therm. **9**, 341 (1997).

[2] O. Pouliquen, J. Delour, and S. B. Savage, Nature **386**,

816 (1997).
[3] Y. Forterre, and O. Pouliquen, Phys. Rev. Lett. **86**, 5886 (2001).
[4] J. McElwaine, and K. Nishimura, Special Publication of the International Association of Sedimentologists **31**, 135 (2001).
[5] Y. Forterre, and O. Pouliquen, J. Fluid Mecha. **486**, 21 (2003).
[6] B. Turnbull, and J. N. McElwaine, J. Geophys. Res. **113**, F01003 (2008).
[7] J. M. N. T. Gray, and C. Ancer, J. Fluid Mecha. **678**, 535 (2011).
[8] Y. Nohguchi, and H. Ozawa, Phys. D **238**, 20 (2009).
[9] S. Courrech du Pont, P. Gondret, B. Perrin, and M. Rabaud, Phys. Rev. Lett. **90**, 044301 (2003).
[10] K. Hutter, S. B. Savage, and Y. Nohguchi, Ann. Glaciol. **13**, 109 (1989).
[11] Y. Nohguchi, Ann. Glaciol. **13**, 215 (1989).
[12] C. Hartel, E. Meiburg, and F. Necker, J. Fluid Mecha. **418**, 213 (2000).
[13] J. N. McElwaine, Philos. Trans. R. Soc. A **363**, 1603 (2005).
[14] R. Fischer, P. Gondret, B. Perrin, and M. Rabaud, Phys. Rev. E **78**, 021302 (2008).
[15] J. Rotne, S. Prager, J. Chem. Phys. **50**, 4831 (1969).
[16] C. Völtz, W. Pesch, and I. Rehberg, Phys. Rev. E **65**, 011404 (2001).
[17] J. L. Vinningland, O. Johnsen, E. G. Flekkoy, R. Toussaint, and K. J. Maloy, Phys. Rev. Lett. **99**, 048001 (2007).